Journal of JSEM, Vol.12, Special Issue (2012) s163-s169

Influence of Projectile Material Properties on Crater Size and Ejecta of Thick Aluminum Alloy 6061-T6 Targets in Hypervelocity Impact

Masahiro NISHIDA[1], Shinji YAMAMOTO[1], Koichi HAYASHI[1] and Sunao HASEGAWA[2]

[1] Graduate School of Engineering, Nagoya Institute of Technology, Gokiso-cho, Showa-ku, Aichi, 466-8555, Japan
[2] Institute of Space and Astronautical Science, Japan Aerospace Exploration Agency, 3-1-1 Yoshinodai, Chuou-ku, Sagamihara, Kanagawa 252-5210, Japan

(*Received 26 December 2011; received in revised form 25 April 2012; accepted 26 April 2012*)

Abstract
The effects of projectile material properties on crater shape and ejecta in thick aluminum alloy 6061-T6 targets were investigated at velocities ranging from approximately 0.5 to 6 km/s. The projectile density affected the crater depth, but the projectiles hardness did not affect it. At the impact velocity of 6 km/s, the density of projectiles clearly affected the mass and size of ejecta fragments. The impact velocity clearly affected the diameter of ejecta rings. The ejecta ring diameter of metal projectiles was almost the same.

Key words
High Velocity Impact, Thick Target, Ejecta, Cratering, Aluminum Alloy

1. Introduction

Space debris is orbiting in a low Earth orbit (LEO) at velocities of more than several km/s, and often strikes spacecraft and space stations. The International Space Station is equipped with shields such as the Whipple bumper and stuffed Whipple bumper to protect it against space debris.

Small-sized space debris, which has low kinetic energy, does not perforate the shields of space stations or the outer surfaces of spacecraft and space stations but forms craters on these surfaces. In such cases, materials from the target surface are ejected, and the projectile fragments are widely scattered. These fragments and ejected materials become new debris, as pointed out by Murr and his co-workers [1]. They studied the hypervelocity impacts of projectiles on thick targets and examined the crater formation and impact fragmentation of projectiles experimentally and numerically [2]. The international standardization of test procedures to evaluate spacecraft material ejecta is being promoted [3]. Many studies have been conducted on related phenomena [4, 5]. However, very few studies have been conducted on crater formation and ejecta composition when projectiles strike thick targets [6], whereas numerous studies have analyzed the impacts of projectiles on thin plates. In this study, we investigated the effects of the material properties of projectiles on crater size and ejecta in thick aluminum alloy targets for impact velocities ranging from approximately 0.5 to 6.0 km/s using a two-stage light-gas gun at ISAS/JAXA with a sabot [7]. The diameter and depth of the crater after impact were measured. The ejecta collected from the test chamber were also examined in detail. The witness plates were observed.

2. Experimental Methods

Four types of projectiles with a diameter of 3.2 mm (1/8 inches) made of pure iron, bearing steel (SUJ2), aluminum alloy (2017-T4) and polycarbonate were used. We examined the effects of their mechanical properties on crater size and ejecta. The mechanical properties of projectile materials are listed in Table 1. The densities of pure iron and bearing steel are almost the same and the hardness of bearing steel is ten times greater than that of pure iron. The hardnesses of pure iron and aluminum alloy are similar and the density of pure iron is three times greater than that of aluminum alloy. Pure iron shows shock-induced phase transition [8]. We expected that this transition would affect the crater size and ejecta, but unfortunately the effect was not observed, as shown below. Polycarbonate, which has very low density and Vickers hardness, was used for comparison.

Thick targets (95-mm diameter, 20-mm/30-mm thickness depending on the impact velocity) made of aluminum alloy 6061-T6 were employed. A witness plate (150 mm × 150 mm, 2 mm in thickness) made of copper, C1100P-1/4H, with a hole of 30 mm was placed 50 mm in front of each target as shown in Fig. 1. The ejecta were observed using a high-speed video camera (Shimadzu Corporation, HPV-1 and Vision Research Inc., Phantom V710). After the experiments, the crater shape was measured using a digital microscope (Keyence Corporation, VHX-1000). The size and weight of ejecta collected from the test chamber were measured.

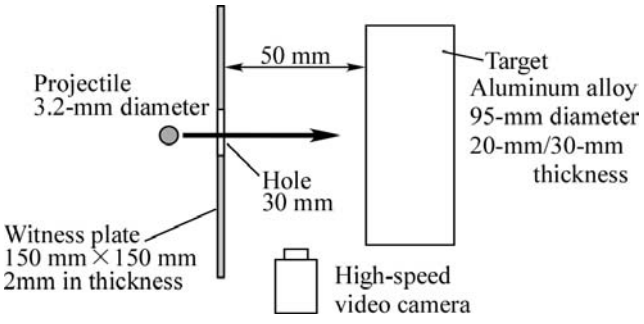

Fig. 1 Experimental setup for hypervelocity impact

Table 1 Mechanical properties of projectile materials

	Vickers hardness	Density [Mg/m^3]	Mass [g] (3.2 mm in diameter)
Pure iron	86	7.9	0.14
Bearing steel, SUJ-2	750-900	7.8	0.13
Aluminum alloy, 2017-T4	118	2.7	0.05
Polycarbonate (PC)	12-13	1.2	0.02

3. Results and Discussion

3.1 Crater size

Fig. 2 shows the measured crater diameter. The diameters of pure iron, bearing steel and aluminum alloy projectiles were almost the same. The results for polycarbonate projectiles were only slightly below those for metal projectiles (pure iron, bearing steel and aluminum alloy). Even though the density and hardness of polycarbonate was much smaller than those of metals, the differences in crater diameter between polycarbonate and metal projectiles were not large.

The crater diameter increased with increasing impact velocity, as expected. In general, the crater diameter is fitted by a power function of impact velocity, $d_c/d_p=aV^m$. Here, d_c is crater diameter, d_p is projectile diameter, V is impact velocity. Walsh and Johnson [9] and Dienes and Walsh [10] suggested m=0.58 for aluminum/ aluminum impacts. Their results of aluminum alloy spheres agree with our results. Charters and Summers [11], Atkins [12], Christman and Gehring [13], and Riney and Heyda [14] used m=2/3 assuming a hemispherical crater shape. However, the values of m for pure iron spheres and polycarbonate spheres were close to 0.75 and 0.5, respectively.

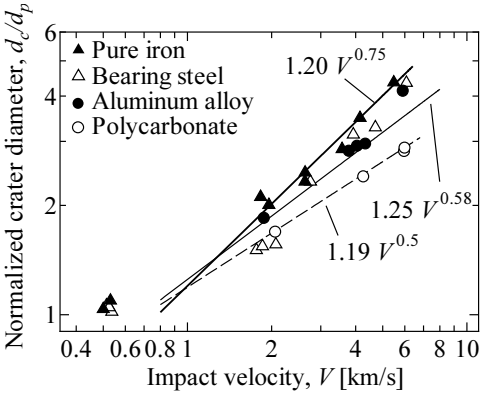

Fig. 2 Comparison of crater diameter with impact velocity

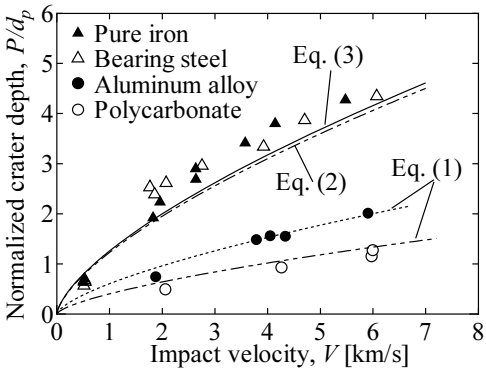

Fig. 3 Comparison of crater depth with impact velocity, P is crater depth

Fig. 3 shows the measured crater depth. Predictably, the crater depth also increased with increasing impact velocity. Even though the hardness for bearing steel was greater than that for pure iron, the depths for pure iron projectiles and bearing steel projectiles were almost the same. The results for aluminum alloy projectiles were below those for pure iron projectiles and bearing steel projectiles. The results for polycarbonate projectiles were below those for aluminum alloy projectiles. JSC equation [15] of eqs. (1) and (2) explains the crater depth.

$$\frac{P}{d_p}=5.24\,{d_p}^{1/18}{H_B}^{-0.25}\left(\frac{\rho_p}{\rho_t}\right)^{0.5}\left(\frac{V}{c_B}\right)^{2/3};\ \text{for}\ \frac{\rho_p}{\rho_t}<1.5 \quad (1)$$

$$\frac{P}{d_p}=5.24\,{d_p}^{1/18}{H_B}^{-0.25}\left(\frac{\rho_p}{\rho_t}\right)^{2/3}\left(\frac{V}{c_B}\right)^{2/3};\ \text{for}\ \frac{\rho_p}{\rho_t}>1.5 \quad (2)$$

Here, P is the crater depth, H_B is the Brinell hardness of the target, ρ_p is the projectile density, ρ_t is the target density, and c_B is the velocity of the bar wave of the target. H_B, ρ_t and c_B of target are 96.8, 2.7 Mg/m^3 and 5030 m/s, respectively. The JSC equation shows that, among the main factors affecting the crater depth, the only significant factor among the material properties of the projectile is the projectile density. In Fig. 3, the crater depths of pure iron and bearing steel were almost the same even though their hardness is different. The crater depth increased with projectile density. We predicted from the experimental results that only the projectile density affected the crater depth, while the projectile hardness did not. The main reason for this is that, in this impact velocity range, the projectile fragmentation occurred. This experimental result agrees with the prediction made using the JSC equation of eq. (1). Because of density difference, GM-DRL equation [16] of eq. (3) was plotted for projectiles of pure iron and bearing steel in Fig. 3 using the maximum of Brinell hardness, H_{BMAX}=110 for aluminum alloy 6061-T6, as well as eq. (2) of JSC.

$$\text{GM-DRL:}\quad \frac{P}{d_p}=2.05\left(\frac{\rho_p^2}{\rho_t}\right)^{0.5}\left(\frac{V^2}{H_{BMAX}}\right)^{1/3} \quad (3)$$

In Fig. 3, the predictions of eqs. (2) and (3) were slightly smaller than the experimental results of pure iron projectiles and bearing steel projectiles.

Fig. 4 shows the aspect ratio of the crater. The aspect ratio of pure iron and bearing steel was almost the same apart from the results at an impact velocity of 2 km/s. It seems that near the velocity of 2 km/s, the result of bearing steel showed anomalous hump which dense, strong projectiles exhibit in plots of crater depth/crater diameter ratio, P/d_c, versus impact velocity in part because of projectile fragmentation or fragmentation onset at impact velocities ranging from about 1 to 2 km/s [1]. The aspect ratio of pure iron projectiles and bearing steel projectiles approached unity as the impact velocity increased. The aspect ratio of aluminum alloy projectiles and polycarbonate projectiles approached 0.5. The main reason for the difference between 1.0 for pure iron projectiles and bearing steel projectiles and 0.5 for aluminum alloy projectiles and polycarbonate projectiles is projectile density, as pointed out by Murr *et al*. [1, 2]. Fig. 5 shows the comparison of the crater shape profiles between the pure iron projectile and the bearing steel projectile. At the velocities of 1.77-1.86 km/s, the crater shape of bearing steel projectiles was narrower and deeper. At the velocities of 2.7 and 4 km/s, the diameter and depth of bearing steel projectile were almost the same as those of pure iron

projectile. The effect of projectile hardness on crater shape decreased with increasing impact velocity.

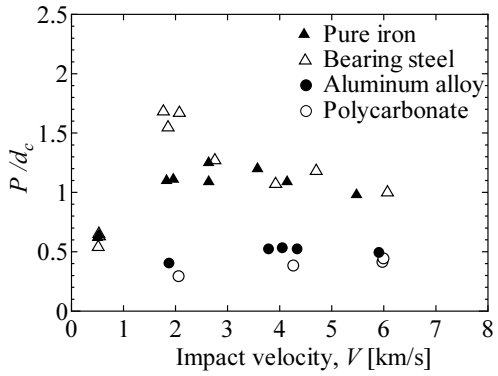

Fig. 4 Aspect ratio of crater shape, P is crater depth and d_c is crater diameter

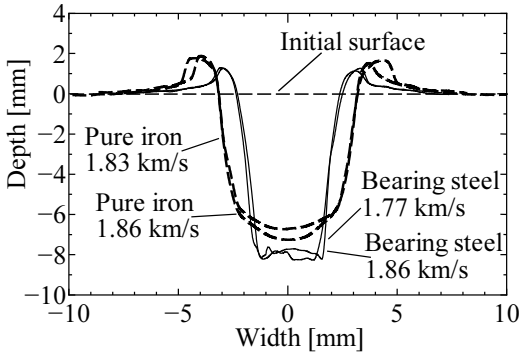

(a) 1.9 km/s

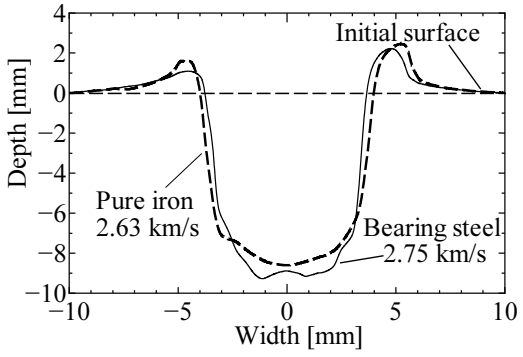

(b) 2.7 km/s

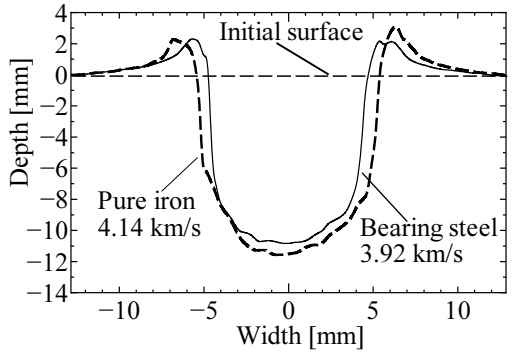

(c) 4.0 km/s

Fig. 5 Comparison of crater shape between pure iron projectile and bearing steel projectiles

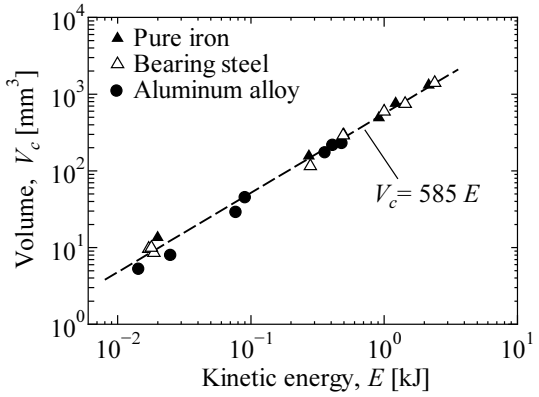

Fig. 6 Comparison of crater volume with initial kinetic energy of projectile

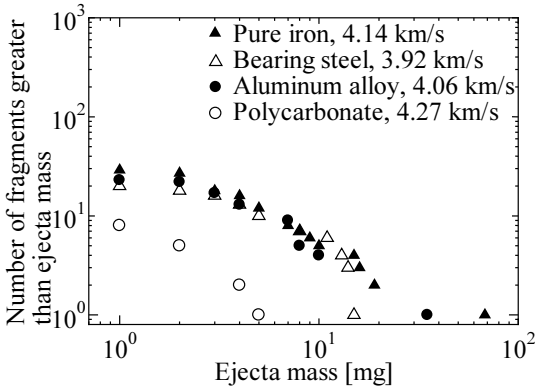

(a) Impact velocity of 4 km/s

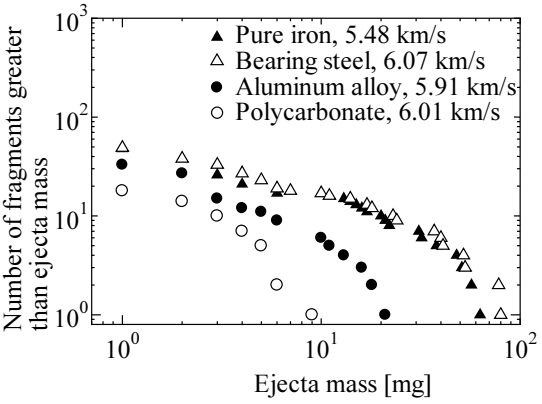

(b) Impact velocity of 6 km/s

Fig. 7 Effect of projectile materials on ejecta mass

For confirmation, Fig. 6 shows the measured crater volume as a function of the initial kinetic energy of the projectile. As expected, the crater volume increased with the initial kinetic energy of the projectile, regardless of the projectile hardness and projectile density. The crater volume of the polycarbonate projectile was too small. It was difficult to measure it accurately.

3.2 Mass of ejecta collected from test chamber

All the ejecta fragments from the targets and all the projectile fragments were collected from the test chamber after the impact experiments. We examined the cumulative number distribution of ejecta mass, which means the number of ejecta fragments with a mass greater than the mass of ejecta fragments on the horizontal axis. Fig. 7(a)

shows the results at an impact velocity of 4 km/s. When polycarbonate projectiles were used, the number of ejecta was much smaller than was the case with metal projectiles. Among metal projectiles, a clear tendency was not observed. Even though we can find the difference in crater depth of aluminum alloy projectiles and pure iron projectile in Fig. 3(b), we cannot find any difference in ejecta mass distribution between aluminum alloy projectiles and pure iron projectile in Fig. 7(a). It is difficult to explain the results in Fig. 7(a) only using the density and/or hardness of projectiles. It seems that the ejecta formation depends on the shape of transient crater, which means cratering process during projectile penetration. Fig. 7(b) shows the results at an impact velocity of 6 km/s. The mass of the collected ejecta is large and a clear tendency was observed. The mass distribution of pure iron projectiles and bearing steel projectiles was almost the same. The cumulative figure for mass when impacted by aluminum alloy projectiles was smaller than those for pure iron projectiles and bearing steel projectiles. Here, because the collected ejecta were too small and too light when impact velocity was less than 3 km/s, the mass distribution could not be examined under 3 km/s.

3.3 Size of ejecta collected from test chamber

The size (length a, width b, thickness c) of ejecta defined in Fig. 8, were measured. Figs. 9(a)-(b) show the cumulative number distribution of ejecta length, a, at an impact velocity of 4 km/s and 6 km/s. At the impact velocity of 4 km/s, no clear tendency was observed, as with the results of mass distribution of ejecta. At the impact velocity of 6 km/s, a clear tendency could be observed. The distribution of pure iron projectiles and bearing steel projectiles were almost the same. The maximum ejecta size and the cumulative number distribution of aluminum alloy projectiles were slightly smaller than was the case with pure iron projectiles and bearing steel projectiles. This tendency was also observed in the results of the characteristic length, $L_c=(a+b+c)/3$, of ejecta using the measured ejecta size, a, b and c, as shown in Fig. 10. The slope of characteristic length distribution was $V^{-1.71}$ of NASA's break up model [17]. As indicated in Figs. 9(b) and 10(b), at the impact velocity of 6 km/s, the ejecta size clearly depends on the kinetic energy of the projectiles, in this case, the density of projectiles, because the impact velocity and the size of projectiles were the same.

The axial ratios, b/a and c/a, of ejecta at the impact velocities of 4 km/s and 6 km/s, are shown in Figs. 11 and 12. The vertical axes in Figs. 11 and 12 represent the cumulative number distribution of the axial ratios of ejecta.

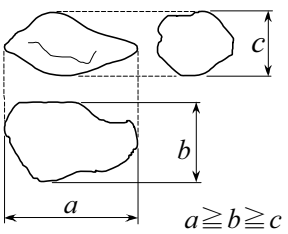

Fig. 8 Definition of ejecta size

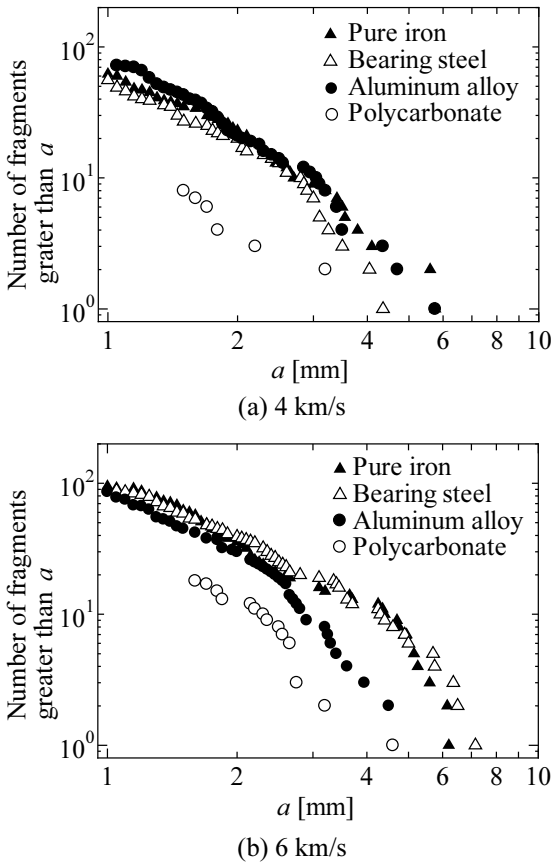

Fig. 9 Ejecta length distribution

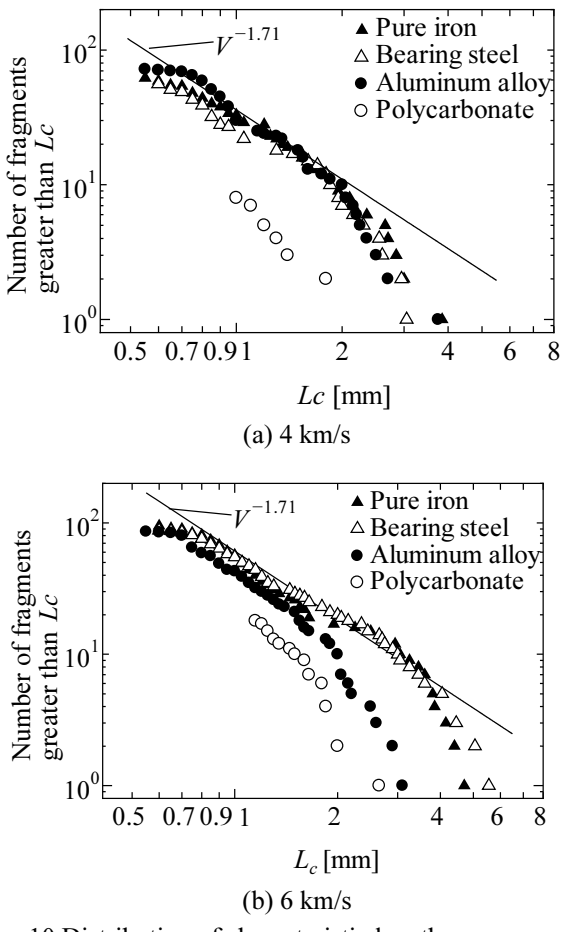

Fig. 10 Distribution of characteristic length

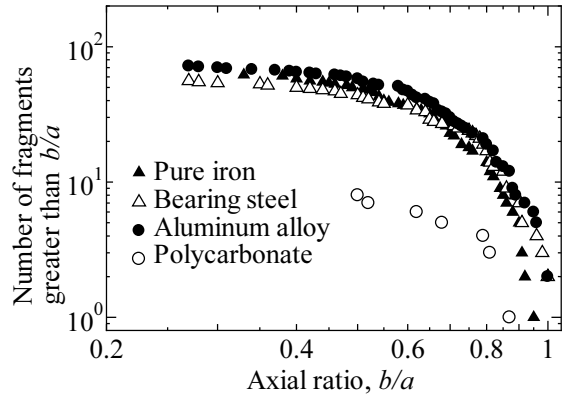

(a) b/a

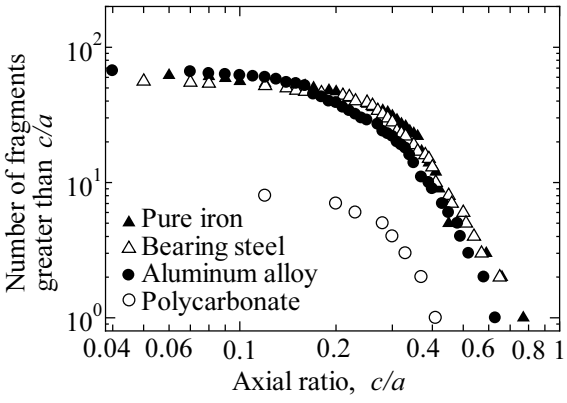

(b) c/a

Fig. 11 Axial ratio of ejecta at impact velocity of 4 km/s

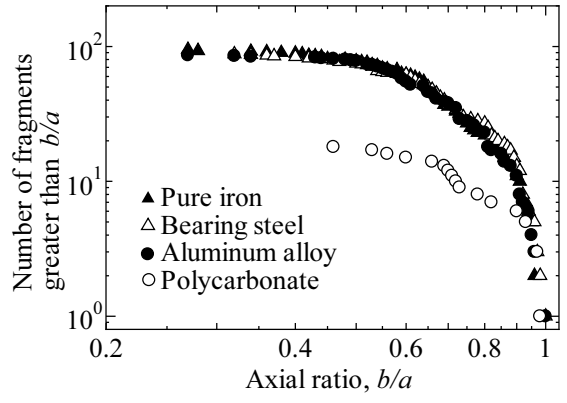

(a) b/a

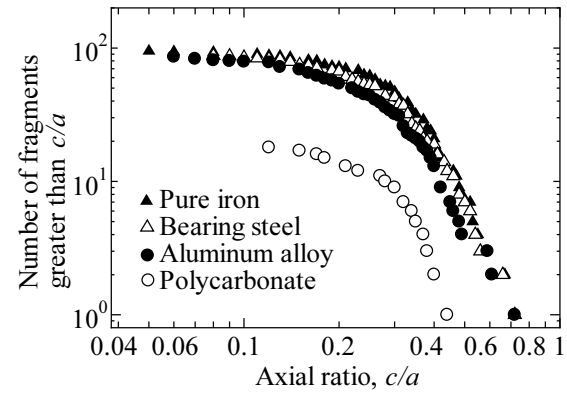

(b) c/a

Fig. 12 Axial ratio of ejecta at impact velocity of 6 km/s

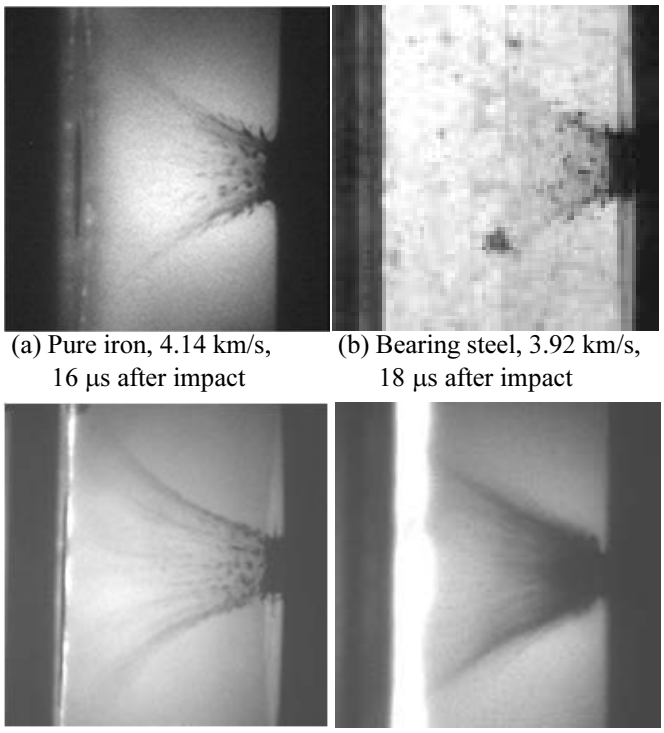

(a) Pure iron, 4.14 km/s, 16 μs after impact

(b) Bearing steel, 3.92 km/s, 18 μs after impact

(c) Aluminum alloy, 4.06 km/s, 16 μs after impact

(d) Polycarbonate, 4.27 km/s, 16 μs after impact

Fig. 13 Effect of mechanical properties of projectiles on ejecta cloud shape, 4 km/s

The distribution of b/a and c/a for polycarbonate projectiles was different from that for metal projectiles. The ejecta induced by the polycarbonate show that c/a is always less than 0.5 at the impact velocities of 4 km/s and 6 km/s. Regardless of impact velocity, the tendency of b/a and c/a for metal projectiles was almost the same. It seems that the axial ratios did not depend deeply on the mechanical properties of metal projectiles or the kinetic energy of projectiles. However, the main reason for this is still unclear, and more detailed investigation into ejecta formation is required.

3.4 Shape of ejecta cloud

To consider the adequacy of the above discussion, the shape of the ejecta cloud was captured using a high speed video camera. Fig. 13 shows the effect of mechanical properties of the projectiles on the shape of the ejecta cloud. The photographs were taken 16 μs/ 18 μs after impact. The ejecta scattered widely into a cone shape. The shape of the ejecta cloud was almost the same among the four types of projectiles. It was also confirmed from the images that the ejecta hit the witness plates

3.5 Observation of witness plates

Images of the witness plates after the experiments are shown in Fig. 14. We observed rings consisting of many indentations (white indentations). In addition to these, outside of the ring we could observe small radial indentations.

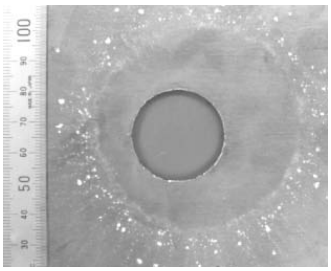

(a) Pure iron, 4.14 km/s

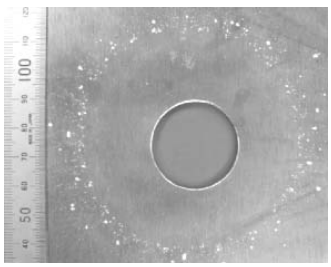

(b) Bearing steel, 3.92 km/s

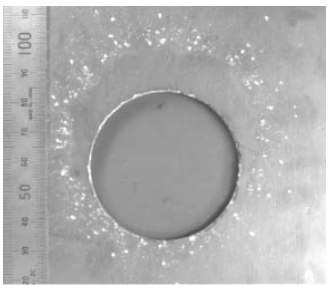

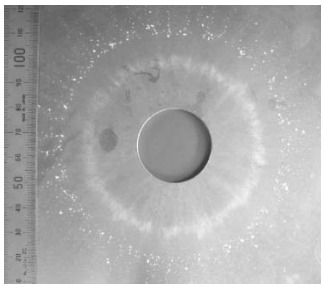

(c) Aluminum alloy, 4.06 km/s (d) Polycarbonate, 4.27 km/s

Fig. 14 Observation of indentation on witness plates (impact velocity: 4 km/s)

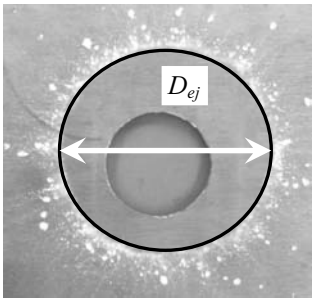

Fig. 15 Definition of ejecta ring diameter, D_{ej}

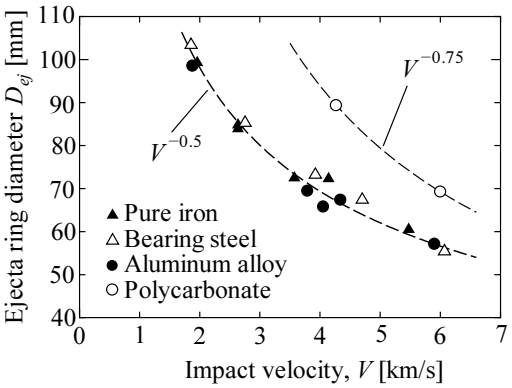

Fig. 16 Impact velocity dependence of ejecta ring diameter

The scatter area of the ejecta was examined. The ejecta ring diameter, D_{ej}, defined in Fig. 15 was measured. Fig. 16 shows that the ejecta ring diameter decreased exponentially with increasing impact velocity. We presumed that the angle of crater wall affected the ejecta ring diameter. When the aluminum alloy projectiles were used, the maximum angles of crater walls were 76° at the impact velocity of 2 km/s and 79° at the impact velocity of 6 km/s, respectively. Here, the angles of crater wall were calculated from the initial surface of target. 90° means the direction perpendicular to the initial surface. The magnitude relationship of the maximum angle of crater wall was in good agreement with that of the ejecta ring diameter. It is possible that the impact velocity dependency of the ejecta ring diameter could be expounded using the maximum angle of crater wall.

The results of curve fitting were also drawn in Fig. 16. The ejecta ring diameter of pure iron projectiles, bearing steel projectiles and aluminum alloy projectiles were almost the same. The ejecta ring diameter of polycarbonate projectiles was larger than that for metal projectiles. When the angles of crater wall were measured, the maximum angles of crater wall for polycarbonate projectiles and bearing steel projectiles were 73° and 88° at the impact velocity of 6 km/s, respectively. Because the ejecta ring diameter of polycarbonate projectiles was larger than that of aluminum alloy projectiles and the maximum angle of crater wall of polycarbonate projectiles was smaller than that of aluminum alloy projectiles, the results of ejecta ring diameter could be expounded using the maximum angle of crater wall. However, even though the ejecta ring diameter of aluminum alloy projectiles was almost the same as that of bearing steel, the maximum angle of crater wall of bearing steel projectiles was larger than that of aluminum alloy projectiles. It is difficult to expound on the results of ejecta ring diameter using the maximum angle of crater wall. It is highly possible that another factor or the angle of "transient" crater wall, which is not final crater wall as discussed above, affected the ejecta ring diameter. More detailed investigation into crater shape (crater wall angle) and ejecta formation is required.

4. Conclusions

The density of the projectiles clearly affected the crater depth, as expected. The density of the projectiles also affected the aspect ratio of the crater shape. At the impact velocity of 6 km/s, the density of the projectiles clearly affected the cumulative number distribution of mass and size. It seems that the density of the projectiles does not affect the cumulative number distribution of axial ratio, b/a and c/a. The ejecta ring diameter decreased with increasing impact velocity. The ejecta ring diameter of the metal projectiles was almost the same. The ejecta ring diameter of polycarbonate projectiles was larger than that of metal projectiles.

Acknowledgement

This work was supported by the Space Plasma Laboratory, ISAS, JAXA. The authors are greatly indebted to Mr. Nobuie Konishi of Nobby Tech. Ltd. for his help with taking images using high speed cameras and to Keyence Corporation for helps with obtaining crater shape profiles using digital microscopes, VHX-2000. This work was supported in part by a Grant-in-Aid for Scientific Research (C), KAKENHI (22560078), from the Japan Society for the Promotion of Science (JSPS).

References

[1] Valerio-Flores, O.L., Murr, L.E., Hernandez, V.S. and Quinodes, S.A.: Observations and Simulations of the Low Velocity-to-hypervelocity Impact Crater Transition for a Range of Penetrator Densities into Thick Aluminum Targets, *J. Mater. Sci.*, **39** (2004), 6271–6289.

[2] Hernandes, V.S., Murr, L.E. and Anchondo, I.A.: Experimental Observations and Computer Simulations for Metallic Projectile Fragmentation and Impact Crater Development in Thick Metal targets, *Int. J. Impact Eng.*, **32** (2006) 1981–1999.

[3] Space Systems-Test Procedures to Evaluate Spacecraft Material Ejecta upon Hypervelocity Impact (ISO-CD-11227).

[4] Sugahara, K., Aso, K., Akahoshi, Y., Koura, T. and Narumi, T.: Intact Measurement of Fragments in Ejecta due to Hypervelocity Impact, *Proc. 60th Int. Astronautical Cong.*, (2009) IAC-09-A6.3.06.

[5] Siguier, J.M. and Mandeville, J.C.: Test Procedures to Evaluate Spacecraft Materials Ejecta upon Hypervelocity Impact, *Proc. IMechE G* **221** (2007) 969–974.

[6] Numata, D., Kikuchi, T., Sun, M., Kaiho, K. and Takayama, K.: Experiment Study of Ejecta Composition in Impact Phenomenon, *Shock Waves*, (2007) Part X.

[7] Kawai, N., Tsurui, K., Hasegawa, S. and Sato, E.: Single Microparticle Launching Method Using Two-stage Light-gas Gun for Simulating Hypervelocity Impacts of Micrometeoroids and Space Debris, *Rev. Sci. Instrum.*, **81** (2010), 115105, 1-4.

[8] Duvall, G. E. and Graham, R. A.: Phase Transitions Under Shock-wave Loading, *Rev. Mod. Phys.*, **49** (1977), 523-579.

[9] Walsh, J.M. and Johnson, W.E.: On the Theory of Hypervelocity Impact, *Proc. 7th Hypervelocity Impact Symp.*, Vol. II, Martin Company (1965), 1-75.

[10] Dienes, J.K. and Walsh, J.M.: Theory of Impact: Some General Principles and the Method of Eulerian Codes, *High Velocity Impact phenomena*, edited by R. Kinslow, (1970), 46-103.

[11] Charters, A.C. and Summers, J.L.: High Seed Impact of Metal Projectiles in Targets of Various Materials, *Proc. 3nd Symp. on Hypervelocity Impact*, Armour Research Foundation, Chicago, Illinois (1959).

[12] Atkins, W.W.: Hypervelocity Penetration Studies, *Proc. 4th Symp. on Hypervelocity Impact*, Vol. 1, Eglin Air Force base, Florida (1960).

[13] Christman, D.R. and Gehring, W.J.: Penetration mechanisms of high velocity projectiles. *Proc. 7th Hypervelocity Impact Symp.*, Vol. VI, Martin Company, (1965).

[14] Riney, T.D. and Heyda, J.F.: Hypervelocity impact calculations, *Proc. 7th Hypervelocity Impact Symp.*, Vol. II, Martin Company, (1965).

[15] Christiansen, E. L.: Handbook for Designing MMOD Protection, NASA/TM-2009-214785 (2009), 34.

[16] Christman, D. R.: Target Strength and Hypervelocity Impact, *AIAA J.*, **4** (1966), 1872-1874.

[17] Johnson, N.L., Krisko, P.H., Liou, J.-C. and Anz-Meador, P. D.: NASA's New Breakup Model of Evolve 4.0, *Adv. Space Res.*, **28** (2001), 1377-1384.